Effect of Titanium Content on Microstructure and Wear Resistance of Fe-Cr-C Hardfacing Layers

By adding different amounts of ferrotitanium into flux cored wire, a hardfacing layer with good performance was obtained, and the M_7C_3 carbide refinement mechanism is discussed

BY Y. F. ZHOU, Y. L. YANG, D. LI, J. YANG, Y. W. JIANG, X. J. REN, AND Q. X. YANG

ABSTRACT

Layers of Fe-Cr-C hardfacing material containing various amounts of titanium were deposited on ASTM 1045 steel base metal. Optical microscope (OM), field emission scanning electron microscope (FESEM) with energy-dispersive spectrometer (EDS), and X-ray diffraction (XRD) were used to investigate the effect of titanium content on the microstructural characteristics of Fe-Cr-C hardfacing layers. The solidification sequence calculation and lattice misfit theory were employed to discuss the M_7C_3 carbide refinement mechanism. The experimental results show the microstructures of Fe-Cr-C hardfacing layers consist of primary $(Cr, Fe)_7C_3$ carbides and the eutectic phases (γ-Fe+$(Cr, Fe)_7C_3$). In the solidification process, the formation and growth of the primary $(Cr, Fe)_7C_3$ carbides occur along their long axis, which parallels the direction of heat flow. With the increase of titanium content, the primary $(Cr, Fe)_7C_3$ carbides are refined. However, it is not proper to increase titanium content without limits. When titanium content reaches 1.17 wt-%, its microstructure changes from a hypereutectic form to a hypoeutectic one. The thermodynamic calculation shows MC carbide precipitates prior to M_7C_3 carbide from Fe-C-Cr-Ti alloy. Moreover, the lattice misfit between $(110)_{TiC}$ and $(010)_{Cr_7C_3}$ is 9.257%, which indicates that TiC acting as heterogeneous nuclei of the Cr_7C_3 is medium effective. Therefore, M_7C_3 carbide can be refined significantly.

Introduction

The Fe-Cr-C alloy, well known for its high hardness and excellent wear and corrosion resistance, has been widely applied in harsh working conditions. Many important workpieces, such as hammers in mining and mineral processing, squeezing rolls in cement production, and abrasion-resistant plates in the manufacturing and metallurgy industries, are manufactured from Fe-Cr-C alloy (Ref. 1). The excellent abrasive wear resistance results primarily from the type, morphology, amount, dimension, and distribution of the carbides, while the toughness of the matrix also contributes to the wear resistance (Ref. 2). Fe-Cr-C alloys have been classified into hypoeutectic, eutectic, and hypereutectic structures (Refs. 3–5). Compared with the hypoeutectic one, the hypereutectic Fe-Cr-C alloy is regarded as having better wear resistance, because its microstructure consists of primary M_7C_3 carbide and eutectic ($\gamma+M_7C_3$) (Ref. 6). While the primary carbides in the hypereutectic microstructure maintain their forms as coarser and larger blocks, this in turn decreases the cast ability (Ref. 7). In general, Fe-Cr-C alloys with hypoeutectic microstructures are applied in engineering by the casting method.

Workpieces made of Fe-Cr-C alloy fail through excessive wear over a period of time. Failed workpieces can be remanufactured using a hardfacing method. Normally, the hardfacing layers are expected to be hypereutectic microstructures for obtaining higher hardness and better wear resistance (Ref. 8). Much attention has been focused on improving the wear resistance of hypereutectic Fe-Cr-C alloys (Refs. 8–12).

Tungsten carbide (WC), acting as an advanced ceramic material with wear resistance and good thermal shock resistance, has been widely used for wear-resistance applications. Kambakas tried to use a double casting technique to produce a WC-particle-reinforced high-Cr white cast iron, and informed that the wear resistance of the high-Cr white cast iron with WC particle reinforcement was significantly better than that without the strengthening phase. For hardfacing consumables, WC particles are not suitable for reinforcing Fe-Cr-C alloy due to the high temperature of the weld pool (Ref. 9).

The applications of rare earth (RE) elements have been of much concern recently because of their excellent properties. By adding RE elements to steel, the crystal grain can be refined. Hao explored the effect of RE oxides on the morphology of carbides in hardfacing metal of high-chromium cast iron. In his studies, the volume fraction and roundness of the carbides were gradually increased, while their area and perimeter were gradually reduced. The carbides were refined and spheroidized, with the RE oxide additions increasing. Nevertheless, the relationship between the volume fraction of carbides and the wear resistance of the hardfacing metal was not established in

Y. F. ZHOU (yef.zhou@gmail.com), *Y. L. YANG, D. LI, J. YANG, Y. W. JIANG, and Q. X. YANG* (qxyang@ysu.edu.cn) *are with State Key Laboratory of Metastable Materials Science & Technology, Yanshan University, Qinhuangdao, China. LI is also with School of Material Science and Engineering, Southwest Jiaotong University, Chengdu, China. X. J. REN is with School of Engineering, Liverpool John Moores University, Liverpool, UK.*

KEYWORDS

Carbides
Hardfacing
Microstructure
Nucleation
Titanium

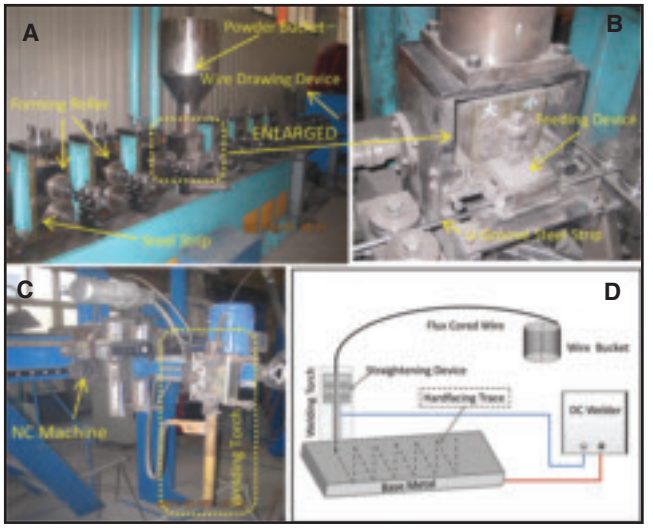

Fig. 1 — A, B — Diagram of flux cored wire fabrication; C — hardfacing equipment; D — hardfacing process.

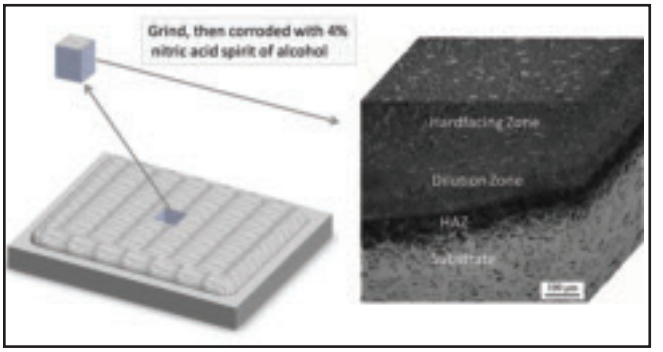

Fig. 2 — Schematic diagram of analysis layer.

his work (Ref. 10).

Vanadium (V), niobium (Nb), and titanium (Ti) are strong carbide-forming elements, and are of benefit for refining the microstructure and improving the wear resistance of the Fe-Cr-C alloy. Qi investigated the effects of vanadium additive on structural properties and tribological performance of high-chromium cast iron hardfacing metal. In his study, V was a benefit element of the Fe-Cr-C alloy. With the addition of V, vanadium carbide was formed as a secondary carbide of Fe-Cr-C-V alloy. The microstructure of the alloy was obviously refined with the increase of V additive, and the amount of bulk primary carbide was reduced with an increase in refined eutectic carbide (Ref. 8). While the carbides in the Fe-Cr-C alloy apparently could also be refined with the Nb addition, the shape of the primary M_7C_3 carbides became isotropic. Via the XRD and EDS analyses, NbC carbide was identified when the Nb element was added into the Fe-Cr-C alloy (Ref. 11).

The contribution of Ti to the Fe-Cr-C alloy also can be found in the literature, but the views contained therein have not yet fully become the consensus. Chung found the added titanium in the Fe–25wt-%Cr–4wt-%C alloy did not act as an inoculant to refine primary M_7C_3 carbides (Ref. 12). Instead, it was just the reverse, as Zhi explained that the heterogeneous nuclei role of TiC in the Fe-Cr-C alloy (Refs. 13, 14). Moreover, the wear resistance of Fe-Cr-C alloy related to the mass fraction of the carbide with added Ti was not quantified as described in previous literature.

Based on the above study, the effect of titanium on hardfacing metal of Fe-Cr-C alloy is reinvestigated in this work. The variation of microstructure, phase transformations, and wear resistance are observed, the carbide refinement under different Ti content is described quantitatively, and the carbide refinement is discussed.

Experimental Procedures

The base metals (100 × 80 ×10 mm) for hardfacing were prepared from ASTM 1045 steel plates. Before welding, the base metals were ground and cleaned with acetone. Flux cored wire, which consisted of an outer steel strip and wrapped powder, was prepared. H08A was selected as the steel strip due to its good toughness. In addition, the composition of the wrapped powder was adjusted by adding different raw materials. The graphite (2 wt-%), ferrochrome (25 wt-%), ferrosilicon (3 wt-%), ferromanganese (3 wt-%), and ferrotitanium were uniformly mixed and prepared. Moreover, to investigate the effect of titanium on the microstructures of the hardfacing layers, 0, 1, 2, and 4 wt-% ferrotitanium, respectively, were also added to the powder. After the powder was prepared, the forming roller was used to roll the steel strip into a U-groove, and then, before the steel strip was rolled into a tubular shape, the well-mixed powder was filled into the U-groove. Furthermore, the required dimension of the flux cored wire was achieved by rolling or wire drawing methods. The diagram of flux cored wire fabrication is shown in Fig. 1A, B.

The bead-on-plate technique with flux cored arc welding (FCAW) was used to deposit the layers via an automated system in which the welding torch was moved back and forth above the base metal at a constant speed in a multitrack overlapping process. The length of the single track was 50 mm, and the overlap width was 4 mm. To reduce the effect of base metal on the microstructure and property of the hardfacing metal, the hardfacing claddings were welded in three layers. Table 1 presents the range of welding conditions, and the hardfacing equipment and process used in this research are shown in Fig. 1C, D.

The center of the hardfacing layers was selected as the analytical region. Specimens were machined into cuboids (10 × 10 × 18 mm) by a wire cutting machine for analysis. The chemical composition of the layers was determined by a SPECTROMAXx optical emission spectrum (OES), and the data are listed in Table 2. Both the horizontal and vertical faces of the specimens were treated with rubdown and polishing processes, and then etched with 4% nitric acid. The microstructures of specimens were observed through an Axiovert 200 MAT optical microscope and a Hitachi S4800 field emission scanning electron microscope (FESEM). The morphology, size, and grade of the primary carbides, and transfer of matrix structures were measured with Image-Pro Plus Version 6.0 software. In addition, 10 OM images were selected randomly from each layer in the horizontal direction at 200× magnification to describe the statistical nature of the maximum diameter and area of each M_7C_3 carbide. The inclusion compositions were analyzed by an EMAX energy-dispersive spectrometer (EDS). D/max-2500/PC X-ray diffraction (XRD) with Cu Kα radiation was used to analyze the constituent phases of the top surface

Table 1 — FCAW Condition

Parameter	Wire Diameter	Voltage	Current	Travel Speed	Welding Layers	Layer Thickness
Value	3.2 mm	22~24 V	240~260 A	300 mm · min^{-1}	3	8 mm

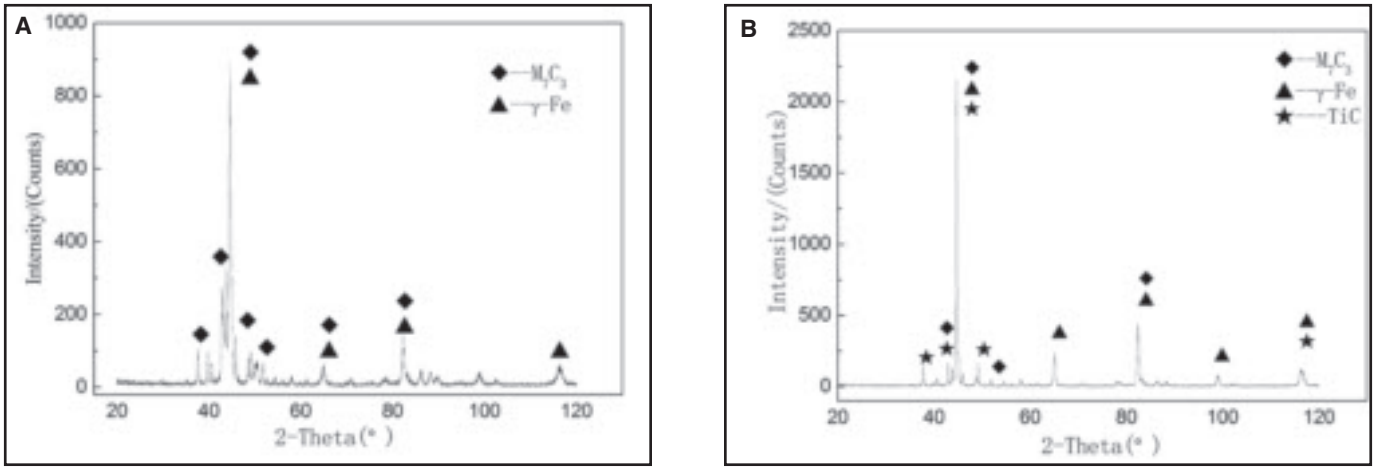

Fig. 3 — XRD of hardfacing layer with and without titanium contents: A — 0 wt-% Ti content; B — 0.28 wt-% Ti content.

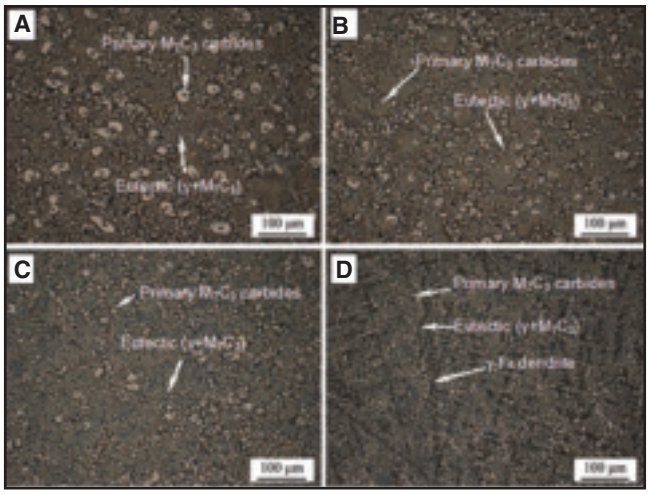

Fig. 4 — OM photographs of Fe-Cr-C-Ti layers in horizontal direction with different titanium contents: A — 0 wt-%; B — 0.28 wt-%; C — 0.63 wt-%; D — 1.17 wt-%.

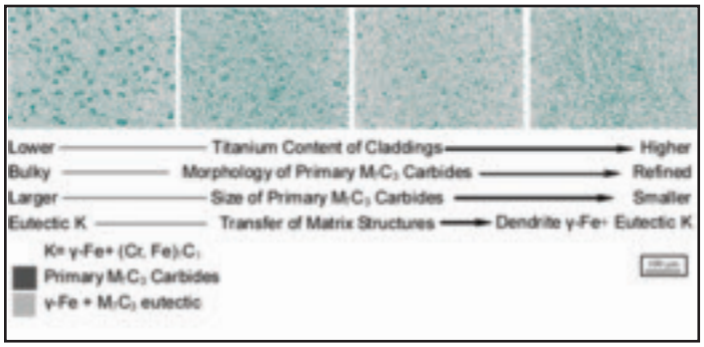

Fig. 5 — Microstructure of Fe-Cr-C-Ti layers with different titanium additions.

of the hardfacing layers. A wear resistance test was conducted on an abrasive belt-type wear testing machine in dry friction. SiC of 80 mesh was selected as the abrasive material, and the wear velocity of the abrasive belt was 1.8×10^4 mm/min. Electronic balance was used in the wear test to weigh the specimens' loss of mass per hour. To decrease experimental error and maintain accuracy, six samples of each chemical composition were prepared for the wear resistance test.

The NETZSCH STA 449 C differential scanning calorimeter (DSC) was used to study the phase transformation of the hardfacing metal. The heating and cooling rates were 40° and 10°C/min, respectively. The Thermo-Calc software was used for phase mass fraction calculation of Fe-Cr-C-Ti alloy with temperature.

Experimental Results and Discussions

Microstructure and Phase Characteristics of the Fe-Cr-C Hardfacing Layers

Figure 2 illustrates the three-dimensional microstructure schematic of the Fe-Cr-C hardfacing layer. The XRD results of surface layers with and without titanium are shown in Fig. 3. From the microscope image of the vertical face, it can be concluded that the specimen can be divided into the hardfacing zone, dilution zone, heat-affected zone (HAZ), and substrate in sequence. With the aid of X-ray diffraction, the hardfacing microstructure with free Ti addition is found to consist of two phases: the primary $(Cr, Fe)_7C_3$ and the eutectic (γ-Fe+$(Cr, Fe)_7C_3$). Besides, after Ti was added into the hardfacing layer, TiC carbide can also be detected in the hardfacing microstructures. Moreover, the microstructure of the dilution zone can be an admixture of γ-Fe, $(Cr, Fe)_7C_3$ and ferrite. The microstructure of the HAZ consists of the coarse grain caused by the heat input

Table 2 — Chemical Compositions of the Hardfacing Layers and Base Metal

	Composition (wt-%)					
Layer	C	Cr	Mn	Si	Ti	Fe
Base metal (1045)	0.43	0.23	0.65	0.21		bal
Specimen a	3.82	16.35	2.24	2.09	0	
Specimen b	3.79	15.97	2.27	2.11	0.28	
Specimen c	3.85	16.14	2.18	2.14	0.63	bal
Specimen d	3.77	16.27	2.22	2.03	1.17	

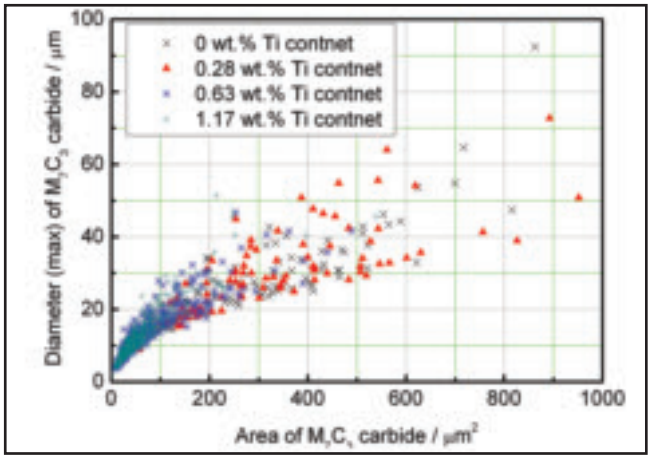

Fig. 6 — Quantitative analysis of M_7C_3 carbide.

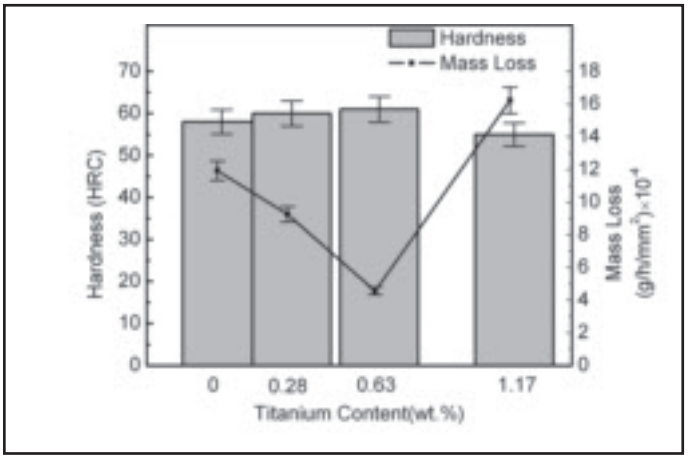

Fig. 7 — Mass loss and hardness of Fe-Cr-C layer with different titanium contents.

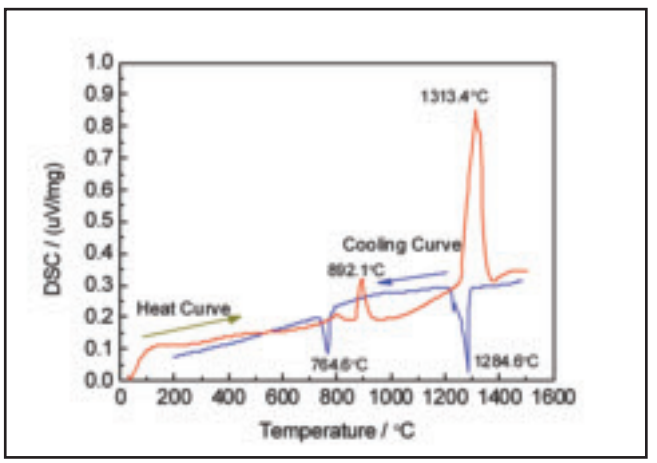

Fig. 8 — Differential scanning calorimeter curves of Fe-Cr-C alloy with 1.17 Ti content.

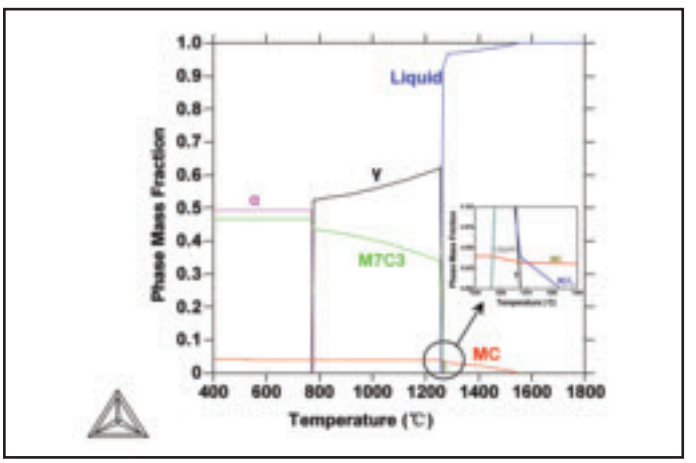

Fig. 9 — Phase mass fraction calculation of Fe-Cr-C-Ti alloy with temperature.

energy, and the substrate contains ferrite. The solidification morphology and the growth pattern of the layer are controlled by the thermal conditions in the weld pool. The formation and growth of the primary $(Cr, Fe)_7C_3$ carbides occur along their long axis, which parallels the direction of the heat flow. The primary $(Cr, Fe)_7C_3$ is the hexagonal-columniation structures. Due to different angles, it is an acicular or blade-like morphology on the vertical faces, and a hexagonal-shaped morphology on the horizontal.

Effect of Titanium on Microstructure of the Fe-Cr-C Hardfacing Layers

For the hardfacing application, the wear resistance is mainly determined by the morphology and distribution of primary $(Cr, Fe)_7C_3$ carbides in the horizontal direction. The OM photographs of the layers in the horizontal direction are shown in Fig. 4.

As shown, the microstructure of the hardfacing layers consisted of primary $(Cr, Fe)_7C_3$ carbides and eutectic (γ-Fe+$(Cr, Fe)_7C_3$), while the carbides and, in particular, the primary carbides, are refined gradually with the increase of Ti content. However, in Fig. 4D, γ-Fe dendrite can be observed. Too much carbon is consumed with the formation of TiC domains when titanium content reaches 1.17 wt-%, resulting in a change in microstructure of the alloy from the hypereutectic form to a hypoeutectic one. Therefore, it is not proper to increase the titanium content without limits.

The schematic diagram of the microstructural changes is illustrated in Fig. 5. As shown, the morphology of primary $(Cr, Fe)_7C_3$ carbides changes from a bulk form to a refined one and the size of primary $(Cr, Fe)_7C_3$ carbides becomes much smaller. Besides, matrix microstructures transform from eutectic (γ-Fe + (Cr,

Table 3 — Planar Lattice Misfit between Orthorhombic Cr_7C_3 and TiC

Matching Interface		$(110)_{TiC}$ //	$(010)_{Cr_7C_3}$
$[uvw]_{TiC}$	[001]	$[\bar{1}10]$	$[\bar{1}11]$
$[uvw]_{Cr_7C_3}$	[001]	[100]	[101]
Θ	0	0	12.1
d_{TiC}(nm)	0.432	0.610	0.747
$d_{Cr_7C_3}$(nm)	0.453	0.701	0.834
δ,%		9.257	

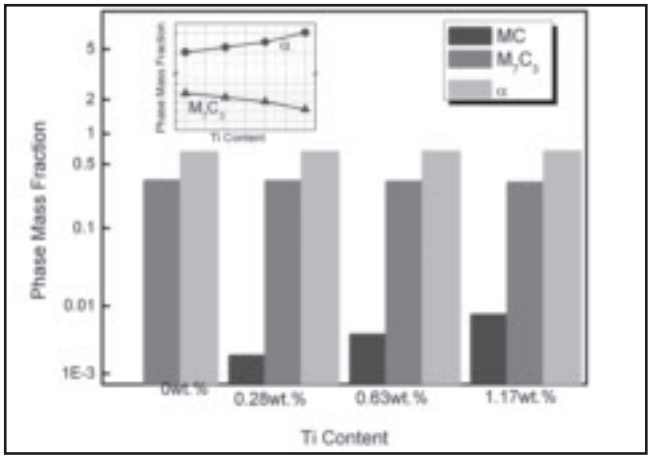

Fig. 10 — Effect of Ti on phase mass fraction calculation of Fe-Cr-C-Ti alloy.

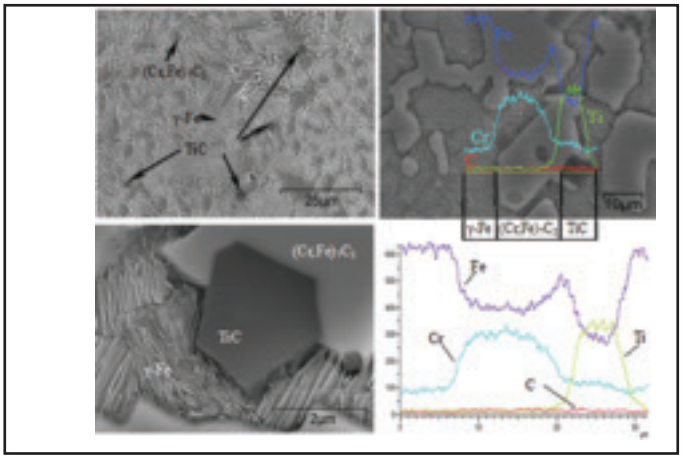

Fig. 11 — FESEM morphology and line scanning results of hardfacing layer.

Fe)$_7C_3$) to dendrite γ-Fe +eutectic (γ-Fe + (Cr, Fe)$_7C_3$).

Because the M_7C_3 carbide is the major reinforcing phase in Fe-Cr-C alloy to reduce friction and wear, the refinement of the carbide was analyzed quantitatively, which is shown in Fig. 6. As shown, the area of M_7C_3 carbide is gradually reduced with the increasing Ti content. When the Fe-Cr-C alloy is Ti-free, the area of M_7C_3 carbide is nonuniform from 200 to 900 μm^2. With higher Ti content, the uniformity of M_7C_3 carbide is enhanced. With 0.28 wt-% Ti content, a majority of M_7C_3 carbide area are distributed between 200 and 600 μm^2 and in the case of 0.63 wt-% Ti content, the M_7C_3 carbide area fell to the range of 100~300 μm^2. As the Ti content increased to 1.17 wt-%, the area of M_7C_3 carbide reduced further, which remained constant at less than 200 μm^2. Besides, the maximum diameter of the M_7C_3 carbide declined markedly as the Ti content increased.

Effect of Titanium on Wear Resistance and Hardness of the Fe-Cr-C Hardfacing Layers

Figure 7 presents the wear resistance and hardness of the hardfacing layers. As illustrated, the wear resistance of the Fe-Cr-C alloy increases and then declines with respect to the amount of added Ti. Meanwhile, the changes in hardness are associated with the wear resistance behavior. When the titanium content is 0.63 wt-%, the Fe-Cr-C hardfacing layer presents the best wear resistance and the highest hardness. There are two factors that lead to the variation in wear-resistance property. TiC carbide, which has a high micro-hardness of 3200–3800 HV (Ref. 15), is present in the Fe-Cr-C alloy as added Ti. However, the high microhardness of TiC carbide may not work to contribute to the improvement in wear resistance. When the Ti content is 1.17 wt-%, the wear resistance behavior is the worst and the hardness has reduced dramatically. Therefore, the TiC carbide itself may not have the main role in the variation of wear-resistance behavior.

Nevertheless, the morphology and distribution of M_7C_3 carbide is changed when Ti is added to the Fe-Cr-C alloy. Particularly when compared with the large block carbide, it has been confirmed that the refined carbide, which has much more contact area with the matrix, causes a better antistripping ability. Therefore, the wear-resistance is better when the carbide is refined and well distributed. However, the M_7C_3 carbide is not only refined but changes its phase structure when too much Ti is added. When the Fe-Cr-C alloy contains 1.17 wt-% Ti, more carbon is consumed to form TiC carbide. The loss of carbon reduces the formation of chromium carbide and causes the hardfacing layer to change from the hypereutectic microstructure to a hypoeutectic one. It is well known that the wear resistance of hypoeutectic Fe-Cr-C alloy without coarse primary carbide is not as good as the hypereutectic alloy, which would lead to a decline in hardness and reduced wear resistance.

Furthermore, the hardness of the hardfacing metal increases from 58 to 61 HRC with the increasing titanium content from 0 to 0.63 wt-%, while the hardness decreases to 55 HRC when the titanium content reaches 1.17 wt-%. The variation in the hardness is consistent with that of the wear resistance results.

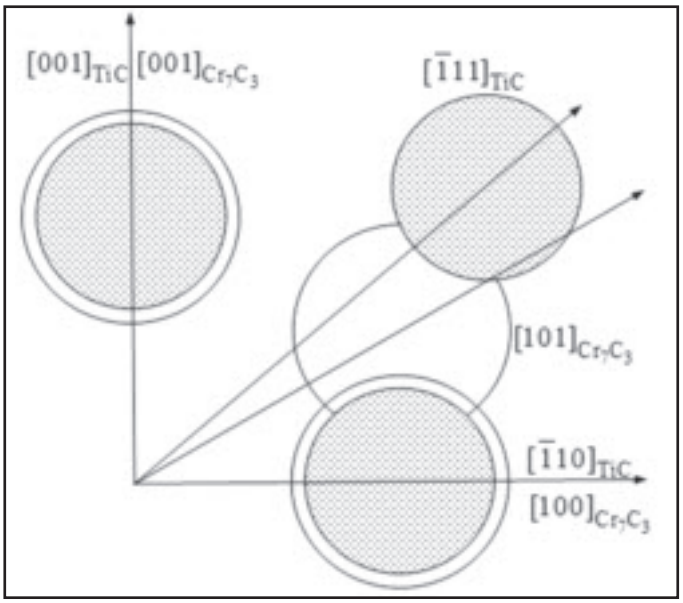

Fig. 12 — Correspondence condition of (110)TiC and (010)Cr_7C_3.

Effect of Titanium on Phase Transformation of the Fe-Cr-C-Ti Alloy

The differential scanning calorimeter (DSC) results for the Fe-Cr-C hardfacing alloy with 1.17 wt-% Ti content are shown in Fig. 8. There are, respectively, two endothermic peaks in the heat process and two exothermic peaks in the cooling process shown in the curves.

The first peak in cooling curve at 1284.6°C is due to the formation of M_7C_3 carbide and γ-phase. And, then, the liquid disappears. At lower temperature, the second exothermic peak can be seen at

764.6°C, corresponding to the transformation from γ-phase to α-phase.

Nevertheless, the MC carbide, whose melting point is higher, cannot be observed in the DSC result. Therefore, the computational thermodynamics method is used to analyze the phase transformation of the Fe-Cr-C-Ti alloy during the equilibrium state. The calculation result is shown in Fig. 9.

The primary phase precipitates from liquid at 1570°C is MC carbide. With the temperature dropping, the MC content is almost invariable and remains at about 0.015 wt-%. At 1280°C, a small quantity of M_7C_3 carbide precipitates from the liquid, and then austenite is expected to form below 1270°C together with some additional precipitation of M_7C_3. At 1260°C, the liquid disappears and the mass fraction of M_7C_3 still increases with a little reduction of austenite. Thereafter, M_7C_3 starts to be transformed from the austenite. When the temperature falls to 780°C, the transformation of austenite to martensite occurs and leads to exotherm in the cooling process. The temperature of exothermic peaks in DSC result (Fig. 8) is close to the calculation, which verifies the exactness of the calculation model.

The influence of titanium on phase mass fraction is shown in Fig. 10. The mass fraction variation of each phase is not obvious during the changes in Ti content. With Ti content increasing, the mass fraction of MC rises slightly. Meanwhile, the mass fraction of M_7C_3 declines because some carbon has been consumed by the Ti content to form the initial MC carbide. Martensite in Fe-Cr-C-Ti alloy ascends slightly due to the rising of austenite at a high temperature.

M_7C_3 Carbide Refinement Mechanism

The results described previously suggest that the improvement in wear resistance is mainly dependent on the refinement of the carbide in Fe-Cr-C-Ti alloy by added Ti content. As an effective element, Ti is widely used in metallurgy of iron and steel for partition to the matrix as well as modification of the carbides (Ref. 14). How it works for refining the Cr_7C_3 carbide is discussed in this section.

Figure 11 shows the field emission scanning electron morphology of the hardfacing layers. From Fig. 11A, it can be seen that square particles are surrounded by $(Cr, Fe)_7C_3$ carbides. According to the EDS analysis and line scanning results of the square particle shown in Fig. 11B and D, the main compositions are titanium and carbon, which indicates that the square particle is TiC carbide. Besides, the more clear morphology of the TiC carbide can be seen in Fig. 11C.

Therefore, it can be said that the refined primary $(Cr,Fe)_7C_3$ carbides are related to TiC carbides. During the hardfacing solidification process, the faster cooling rate results in smaller dimensions and greater number of nuclei. The resistance of heterogeneous nucleation mainly depends on the interfacial energy between nucleation basement and crystalline phase. And the interfacial energy is constituted by its chemistry item and structural one. The chemistry item includes bond strength, bond energy, and bond types between atoms, and the structural item is mainly decided by lattice distortion energy, which is caused by the atomic misfit. Misfit is the major factor of the interfacial energy in higher lattice distortion energy.

The value of the two-dimensional lattice misfit is used to estimate whether some inclusions can act as the heterogeneous nuclei. A mathematical model of the two-dimensional lattice misfit is as follows (Ref. 16):

$$\delta_{\frac{(hkl)_s}{(hkl)_n}} = \sum_{i=1}^{3}\left[\left(\left|d_{[uvw]_s^i}\cos\theta - d_{[uvw]_n^i}\right| / d_{[uvw]_n^i}\right)/3\right]\times 100 \quad (1)$$

Where

$(hkl)_s$ is a low-index plane of the matrix;

$[uvw]_s$ is a low-index direction in $(hkl)_s$;

$(hkl)_n$ is a low-index plane in the nucleated solid;

$[uvw]_n$ is a low-index direction in $(hkl)_n$;

$d_{[uvw]n}$ is the interatomic spacing along $[uvw]_n$;

$d_{[uvw]s}$ is the interatomic spacing along $[uvw]_s$;

θ is the angle between the $[uvw]_s$ and $[uvw]_n$ (θ≤90 deg).

Bramfitt (Ref. 16) proposed a theory regarding the heterogeneous nucleation process. The nuclei with δ<6% is the most effective, and that with δ between 6 and 12% is medium effective, while that with δ>12% is ineffective.

The crystal lattice of TiC is face-centered cubic, and its lattice parameter is a = 0.432 (nm). Orthorhombic Cr_7C_3 is one mode of $(Cr, Fe)_7C_3$, and its lattice parameters are a = 0.701 (nm), b = 1.214 (nm), and c = 0.453 (nm) (Refs. 17, 18). The atom correspondence condition of those two planes is shown in Fig. 12. Table 3 lists the calculated result of the lattice misfit δ between $(110)_{TiC}$ and $(001)_{Cr7C3}$. It can be seen that the lattice misfit between $(110)_{TiC}$ and $(001)_{Cr7C3}$ is 9.257%. According to Bramfitt's two-dimensional lattice misfit theory, TiC acting as heterogeneous nuclei of the Cr_7C_3 is middle effective and the primary Cr_7C_3 carbides are refined. These results are appropriate supplements that some works (Ref. 13) also point out that titanium and/or niobium can refine the microstructure of the Fe-Cr-C alloy.

Conclusions

A series of Fe-Cr-C hardfacing layers with varying amounts of titanium was deposited by the FCAW process. The microstructure and wear resistance of the Fe-Cr-C hardfacing layers were determined and correlated to the varying titanium contents. Meanwhile, the carbide refinement mechanism and the phase precipitation rule were discussed. Following are the major conclusions that can be drawn from this work:

- Microstructures of the hardfacing layers consisted of the primary $(Cr, Fe)_7C_3$ and the eutectic (γ-Fe+$(Cr, Fe)_7C_3$). The existence of M_7C_3-type carbide maintains a high hardness and good wear resistance of the Fe-Cr-C alloy.
- Primary $(Cr, Fe)_7C_3$ carbides are refined gradually with the increase in titanium content. The morphology changes from a bulk form to a refined one. Meanwhile, the increase in hardness and wear resistance improve until the titanium content is increased to 0.63 wt-%. When the titanium content is 1.17 wt-%, too much carbon is consumed by titanium to form TiC carbide. This leads the microstructure of the Fe-Cr-C alloy to change from a hypereutectic form to a hypoeutectic one. In addition, the hardness decreases and wear resistance becomes worse. Therefore, it is not proper to increase the titanium content unlimitedly, and the x%Fe-16%Cr-3.8%C alloy with 0.63 wt-% titanium content is more appropriate.
- The M_7C_3 carbide refinement is related to the complex metallurgical reactions. According to the thermodynamic calculations, the MC carbide is found to precipitate prior to the M_7C_3 carbide. This provides the MC carbide with the chance to act as the heterogeneous nuclei of M_7C_3 carbide. Moreover, the lattice misfit between $(110)_{TiC}$ and $(010)_{Cr7C3}$ is 9.257%, which indicates that TiC acting as heterogeneous nuclei of the Cr_7C_3 is medium effective due to Bramfitt's theory. Therefore, the M_7C_3 carbide can be refined.

Acknowledgments

The authors would like to express their gratitude for projects supported by Program for 100 excellent talents of Hebei Province of China (SPRC 021) and key project of science and technology of Hebei Province (09215106D).

References

1. Jacuinde, A. B., Correa, A. R., and Quezada, J. G. 2005. Effect of titanium on the as-cast microstructure of a 16% chromium white iron. *Materials Science and Engineering A* 398(1-2): 297–308.

2. Llewellyn, R. J., Yick, S. K., and Dolman, K. F. 2004. Scouring erosion resistance of metallic materials used in slurry pump service. *Wear* 256(6): 592–599.

3. Menon, R., and Wallin, J. 2008. Specialty cored wires for wear and corrosion applications. *Welding Journal* 87(2): 31–36.

4. Menon, R. 2002. Recent advances in cored wires for hardfacing. *Welding Journal* 81(11): 53–58.

5. Wiengmoon, A., Chairuangsri, T., Brown, A., and Pearce, J. T. H. 2005. Microstructural and crystallographical study of carbides in 30 wt.% Cr cast irons. *Acta Materialia.* 53(15): 4143–4154.

6. Asensio, J., Pero-Sanz, J. A., and Verdej, J. I. 2003. Microstructure selection criteria for cast irons with more than 10 wt.% chromium for wear applications. *Materials Characterization* 49(2): 83–93.

7. Liu, H. N., Sakamoto, M., and Nomura, M. 2001. Abrasion resistance of high Cr cast irons at an elevated temperature. *Wear* 250(1-12): 71–75.

8. Qi, X. W., Jia, Z. N.,and Yang, Q. X. 2011. Effects of vanadium additive on structure property and tribological performance of high chromium cast iron hardfacing metal. *Surface and Coatings Technology* 205(23-24): 5510–5514.

9. Kambakas, K., and Tsakiropoulos, P. 2005. Solidification of high-Cr white cast iron-WC particle reinforced composites. *Materials Science and Engineering A* 413-414: 538–544.

10. Hao, F. F., Li, D., and Yang, Q. X. 2011. Effect of rare earth oxides on the morphology of carbides in hardfacing metal of high chromium cast iron. *Journal of Rare Earths* 29(2): 168–172.

11. Zhi, X. H., Xing, J. D., and Fu, H. G. 2008. Effect of niobium on the as-cast microstructure of hypereutectic high chromium cast iron. *Materials Letters* 62(6-7): 857–860.

12. Chung, R. J., Tang, X., and Li, D. Y. 2009. Effects of titanium addition on microstructure and wear resistance of hypereutectic high chromium cast iron Fe-25wt.%Cr-4wt.%C. *Wear* 267(1-4): 356–361.

13. Zhi, X. H., Xing, J. D., and Fu, H. G. 2008. Effect of titanium on the as-cast microstructure of hypereutectic high chromium cast iron. *Materials Characterization* 59(9): 1221–1226.

14. Wu, X. J., Xing, J. D., and Fu, H. G. 2007. Effect of titanium on the morphology of primary M_7C_3 carbides in hypereutectic high chromium white iron. *Materials Science and Engineering A* 457(1-2): 180–185.

15. Suzuki, A. 1999. Effect of multiply charged ions on the Vickers hardness of TiC films. *Japanese Journal of Applied Physics* 38: 881–885.

16. Bramfitt, B. L. 1970. The effect of carbide and nitride additions on the heterogeneous nucleation behavior of liquid iron. *Metallurgical and Materials Transactions B* 1(7): 1987–1995.

17. Dennis, W. H., and William, V. G. 2008. Crystallography and metallography of carbides in high alloy steels. *Materials Characterization* 59(7): 825–841.

18. Shtansky, D. V., Nakai, K., and Ohmori, Y. 1999. Crystallography and interface boundary structure of pearlite with M_7C_3 carbide lamellae. *Acta Materialia* 47(4): 1105–1115.

— continued from page 94

and the IIW. His many awards include the AWS Honorary Membership, National Meritorious, Safety and Health, and the Robotic and Automatic Arc Welding. Hinrichs is survived by his wife Patricia and family members. The AWS Milwaukee Section has established the John Hinrichs Memorial Endowment Scholarship. To contribute to to this memorial, contact Vicki Pinsky, *vpinsky@aws.org,* (800/305) 443-9353, ext. 212.

James M. Sawhill Jr.

James M. Sawhill Jr., 71, an AWS Fellow, died suddenly June 1 in James City County, Pa. A native of Baltimore, Md., he was a Maryland state champion wrestler in 1959 and ran the New York City Marathon in a time of 3:30. He received his degree in materials science from North Carolina State University in Raleigh where he was named Outstanding Engineering Senior with a 4.0 average. He received his master's in 1966 from Lehigh University and PhD in materials engineering from Rensselaer Polytechnic Institute in 1972. Sawhill, active with AWS and ASM International, made numerous contributions to the welding and metallurgical fields. He received one patent and published more than 20 technical papers. Because of his passion for the children he befriended while working through Rotary International with the *Refugio de los Sueños* in Quito, Ecuador, the family requests memorials be made to benefit the Jim Sawhill Memorial Project, Yorktown Rotary Foundation, PO Box 142, Yorktown,VA 23690. Sawhill is survived by his wife, Mary, two daughters, two sisters, and a grandson.

James Sawhill Jr.

Frank D. Pigage

Frank D. Pigage, 78, died April 6 in Fort Myers, Fla. He served on the executive board of the AWS Philadelphia Section for many years. Pigage was a welding distributor sales person for more than 20 years with E. R. Joseph Co., in Norristown, Pa. He also worked for the Fisher Tank Co. in Chester, Pa., and BOC Airco in Reading, Pa. Pigage is survived by his wife, Phyllis, three sons, four grandchildren, and a sister.◆

Frank Pigage